JOURNAL OF SPACECRAFT AND ROCKETS
Vol. 38, No. 1, January–February 2001

Transient Coupling of Launch Vehicle Bending Responses with Aerodynamic Flow State Variations

K. W. Dotson*
The Aerospace Corporation, Los Angeles, California 90009-2957

Current analytic formulations for the self-sustained coupling of launch vehicle bending responses with aerodynamic flow state variations are restricted to prediction of the limit cycle state and associated stiffness and damping values. The theory is extended to include evolution of the structural response during transonic flight to the limit cycle state. The method of multiple scales is used to analyze the nonlinear equation of motion. The resulting analytic expressions agree well with histories from a rigorous numerical solution for the idealized force–response coupling relationship. It is shown that the transient response for launch vehicle aeroelastic coupling depends on the initial conditions, the structural frequency and damping, and the time lag associated with flow state changes. It is also shown that the maximum response during the transonic regime can be significantly smaller than that for the limit cycle state, depending on the combination of these variables. In particular, the short time period that launch vehicles typically spend in the transonic regime precludes convergence of the bending mode response to the limit cycle state when the structural frequency and damping are low. The structure of the solution space is described, and it is shown that a subcritical Hopf bifurcation exists when the flow state changes at 0 deg.

Nomenclature

c	=	speed of sound, ft/s
f	=	bending mode natural frequency, Hz
h	=	dissipative and nonlinear terms in differential equation, 1/s
n	=	aerodynamic stiffness, dimensionless
$\dot{n}$	=	aerodynamic damping, dimensionless
r	=	response amplitude, dimensionless
T_0	=	fast time, s
T_1	=	slow time, dimensionless
t	=	time, s
$\ddot{x}$	=	absolute vehicle acceleration, g
z	=	generalized translation normalized with respect to its static value, dimensionless
ΔM	=	Mach number interval, dimensionless
Δt	=	time required for flow state change, s
ε	=	small-valued parameter in series expansion, 1/s
ζ	=	structural damping (as a ratio to the critical value), dimensionless
λ	=	eigenvalue of Jacobian matrix, 1/s
ξ	=	force variation, dimensionless
ϕ	=	phase, rad
ω	=	circular frequency, rad/s

Subscripts

cr	=	critical
e	=	excitation
ic	=	initial condition
l	=	force lag
lc	=	stable limit cycle
p	=	force pulse
u	=	unstable limit cycle
0	=	first term in series expansion
1	=	second term in series expansion

Introduction

THE flow at the cone cylinder junction of a launch vehicle payload fairing can be either attached or separated in the transonic regime. In 1963, it was first observed that the flow can alternate between these states over fixed ranges of Mach number and angle of attack.[1,2] Schlieren photographs from Ref. 1 are shown in Fig. 1, in which the flow on the leeward side of the model changes from an attached to separated state for a 2-deg angle of attack.

The external pressure change that occurs during a flow state transition imposes a force on the launch vehicle. Because the flow alternations depend on the rotation of the payload fairing nose cone, the force and response are coupled. The idealized force–response relationship shown in Fig. 2 was used in Ref. 3 to derive closed-form equations for the fluid–structure interaction. Transonic flight measurements support the steplike force changes depicted in Fig. 2 (Ref. 4).

It is assumed in this model that the flow alternations occur on both sides of the payload fairing as the launch vehicle oscillates, a condition that yields the maximum structural response.[3] Because most launch vehicles fly with an angle of attack close to 0 deg, and because most payload fairing shapes exhibit flow state alternations for small angle-of-attack values, the two-sided alternations are generally representative of flight conditions.[3] It is further assumed that the launch vehicle response can be analyzed as a single-degree-of-freedom system represented by a bending mode generalized coordinate. Launch vehicle aeroelastic coupling belongs, with aircraft wing torsion[5] and control surface buzz,[6] in the class of single-degree-of-freedom problems involving feedback between transonic shock-wave motion and structural responses. A criterion for validity of the single-mode assumption for launch vehicle aeroelastic coupling is provided in Ref. 4.

The equation of motion corresponding to the force–response coupling depicted in Fig. 2 is nonlinear. Numerical solution of this equation shows that, provided the initial condition exceeds a known value, the response converges to a single limit cycle state.[3] Closed-form expressions for the limit cycle amplitude were derived in Ref. 3 based strictly on the steady-state force–response relationship. An alternate approach, used historically for fluid–structure interaction problems, computes constant aerodynamic stiffness and damping coefficients that modify the system frequency and damping.[7] In the current problem, the modified equation of motion could be used in a transient response analysis of the transonic buffeting forces. Closed-form expressions for aerodynamic stiffness and damping coefficients corresponding to launch vehicle aeroelastic coupling were derived in Ref. 7. It was shown that these coefficients linearize the equation of motion, but the approximation is acceptable provided the aeroelastic coupling contribution to the total system response overwhelms that due to buffeting.

The methodology used in Refs. 3, 4, and 7 is semi-empirical because it relies on steady pressure data and a force–response

Received 28 October 1999; revision received 14 September 2000; accepted for publication 16 September 2000.

*Engineering Specialist, Structural Dynamics Department, P.O. Box 92957, M4/909. Senior Member AIAA.

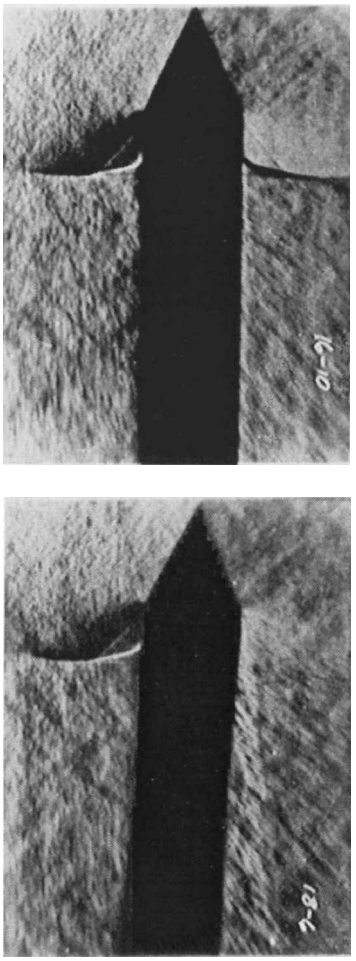

Fig. 1 Schlieren photographs of flow state change observed in wind-tunnel tests for $M_\infty = 0.89$: a) 0-deg angle of attack and b) 2-deg angle of attack (reproduced with permission of Arnold Engineering Development Center[1]).

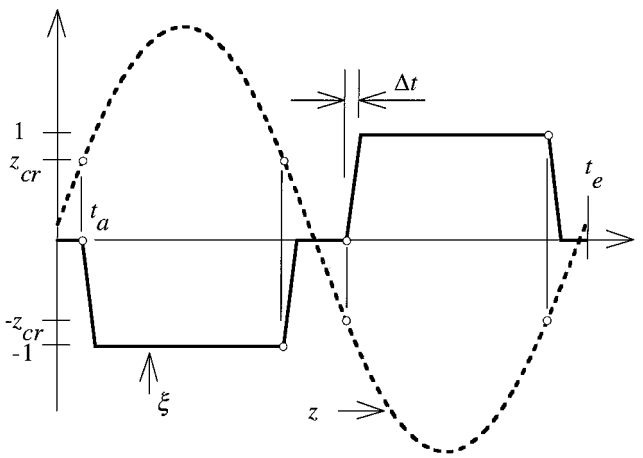

Fig. 2 Schematic of one cycle of coupled force and response in present theory.

idealization to define the unsteady forcing function. Computational fluid dynamics (CFD) methods have also been used to analyze launch vehicle aeroelastic coupling.[8,9] In this approach, the flow solver is coupled to the structural equations of motion. The CFD analysis, however, depends on the accuracy of the aerodynamic formulation and can be computationally intensive. In contrast, the semi-empirical approach can be implemented with a hand calculator and readily identifies the relative importance of the structural and flowfield parameters.

There is a paucity of data that can be used for validation of the CFD and semi-empirical approaches. Flow state changes are evident in Titan IV flight data,[4] but the direction of the resulting external forces precludes aeroelastic instability for this launch vehicle.[4] Also, it does not appear that wind-tunnel tests with an oscillating test article have demonstrated the unsteady coupling of flow state changes with critical response values. Finally, because of the long run times required for convergence of the response to the limit cycle state, and because of uncertainties in modeling the turbulent boundary layer and the fluid–structure interaction that causes flow state changes, the existing CFD results[8,9] are inadequate for validation of the semi-empirical analysis.

It is possible that improvements in the computational speed and accuracy of CFD flow solvers will eventually replace semi-empirical methods. Currently, however, the latter is preferred by industry for analysis of the aeroelastic stability of new launch vehicle configurations. Note that semi-empirical approaches are currently also used for the analysis of aircraft limit cycle oscillation because of CFD limitations.[10]

Semi-empirical studies of the self-sustained coupling of launch vehicle responses with flow state variations have focused on the prediction of the limit cycle state. This work extends the theory to include the evolution of the steady-state response. The force–response coupling relationship shown in Fig. 2 and the analysis assumptions presented in Ref. 3 are used. In this work, however, Fig. 2 corresponds to any given response cycle, not just to the limit cycle state. The phenomenological model provides insight into the mechanisms that predominately define the response evolution and provides a means of estimating the effects of the system parameters.

Transient Force–Response Coupling

The equation of motion for idealized aeroelastic coupling is given by[3]

$$\ddot{z}(t) + 2\zeta\omega\dot{z}(t) + \omega^2 z(t) = \omega^2 \xi(z) \tag{1}$$

in which the bending mode response z has been normalized with respect to its maximum static value and the normalized force term ξ satisfies the relationship shown in Fig. 2. Further details regarding the derivation of the equation of motion and definition of the force amplitude using steady wind-tunnel test data are provided in Ref. 3. Equation (1) is nonlinear because the normalized force term ξ is a function of the displacement z; that is, the deflection value z_{cr}, which is related to the critical nose rotation for the payload fairing geometry,[3] defines the initiation points for flow state changes.

Only forced vibration is addressed in this work. Closed-form expressions for the free vibration response after cessation of steady-state force alternations were developed in Ref. 3. These expressions demonstrate that, after the launch vehicle exits the transonic regime, the response amplitude can be significantly higher than the limit cycle state.

The transient response from Eq. (1) is desired. A numerical solution can be determined by evaluating Eq. (1) given the force–response relationship shown in Fig. 2. An analytic solution, however, is derived herein to provide insight into the evolution of the response to the limit cycle state. Use is made of well-known perturbation methods, which represent the solution z by the first few terms of an asymptotic expansion.[11] The expansion is commonly carried out in powers of a parameter ε that appears naturally in the equation of motion. The expansion consequently has the form

$$z(t;\varepsilon) = z_0(t) + \varepsilon z_1(t) + \varepsilon^2 z_2(t) + \cdots \tag{2}$$

where z_n is independent of ε and $z_0(t)$ is the solution of the problem for $\varepsilon = 0$.

Many variants exist in the class of solutions called perturbation methods. The method of multiple scales was chosen for this application and is described in detail in Ref. 11. The name of the procedure derives from its use of multiple timescales (defined by $T_0 = t$, $T_1 = \varepsilon t$, $T_2 = \varepsilon^2 t$, etc.) to analyze the response amplitude and phase. Provided that $0 \le \varepsilon \le 1$, each successive timescale is slower than the former. In the present application, only T_0 and T_1 are used. Additional timescales, which increase the complexity of the solution, were not necessary because the approximation from two scales agrees well with numerical results.

In the approach, the multiple scales are treated as independent variables. For example, functions of the fast timescale T_0 are constant on the slow timescale T_1. With use of the chain rule, the time derivative is then transformed according to

$$\frac{\mathrm{d}}{\mathrm{d}t} = \frac{\partial}{\partial T_0} + \varepsilon\frac{\partial}{\partial T_1} + \cdots \tag{3}$$

Equation (3) has the effect of converting an ordinary differential equation, such as Eq. (1), into a partial differential equation. Equation (3), furthermore, shows that the approximate solution is obtained by not only expanding the dependent variable z, but also the time derivatives. Hence, the method of multiple scales is also called the derivative-expansionmethod.[11]

Application of the Method of Multiple Scales

Classification of the Forced Excitation

In the current problem, the parameter for the expansion of z is taken as

$$\varepsilon = 2\zeta\omega \tag{4}$$

Equation (1) can then be rewritten as

$$\ddot{z}(t) + \omega^2 z(t) = -\varepsilon\dot{z}(t) + K\xi(z) \tag{5}$$

Because $K = \omega^2 = \mathcal{O}(1)$, excitation from the force term $\xi(z)$ is classified as hard.[11] The perturbation solution for hard excitation depends on the proximity of the forcing and natural frequencies. When $\omega_e - \omega = \mathcal{O}(1)$, the excitation is called nonresonant, whereas $\omega_e - \omega = \mathcal{O}(\varepsilon)$ defines resonance.[11]

In the current problem, because of the dependence of the forcing on the displacement z, a single frequency ω_e does not exist for all time. A classification regarding resonance, however, can be made based on derivations in Ref. 3 for the limit cycle state. With use of these expressions, it can be shown that

$$\omega_e - \omega \cong \omega\left(\sqrt{1 + 2\varepsilon/\omega^2\Delta t} - 1\right) = \mathcal{O}(\varepsilon) \tag{6}$$

as $\varepsilon \to 0$. Therefore, for the purpose of obtaining an approximate solution of Eq. (5), the excitation can be classified as hard resonance. Reference 11 indicates that, in this case, the factor K can be expressed as εk such that

$$\ddot{z} + \omega^2 z = \varepsilon h(z, \dot{z}) \tag{7}$$

$$h = k\xi - \dot{z} \tag{8}$$

where $k = \omega/2\zeta$. Note that the value of k is generally very large because ε is small. Setting ε equal to zero in Eq. (7) reveals that, in the current problem, the method of multiple scales approximates the forced nonlinear response as a perturbation from the undamped free vibration of a linear oscillator with natural frequency ω.

Transformation of Equation of Motion

The expansion of the displacement z will be truncated at two terms such that

$$z = z_0(T_0, T_1) + \varepsilon z_1(T_0, T_1) + \mathcal{O}(\varepsilon^2) \tag{9}$$

The derivative expansion in Eq. (3) yields the following expressions for velocity and acceleration:

$$\dot{z} = \frac{\partial z_0}{\partial T_0} + \varepsilon\left(\frac{\partial z_0}{\partial T_1} + \frac{\partial z_1}{\partial T_0}\right) + \mathcal{O}(\varepsilon^2) \tag{10a}$$

$$\ddot{z} = \frac{\partial^2 z_0}{\partial T_0^2} + \varepsilon\left(\frac{\partial^2 z_1}{\partial T_0^2} + 2\frac{\partial^2 z_0}{\partial T_0 \partial T_1}\right) + \mathcal{O}(\varepsilon^2) \tag{10b}$$

Substituting Eq. (10) into Eq. (7) yields

$$\frac{\partial^2 z_0}{\partial T_0^2} + \varepsilon\left(\frac{\partial^2 z_1}{\partial T_0^2} + 2\frac{\partial^2 z_0}{\partial T_0 \partial T_1}\right) + \omega^2(z_0 + \varepsilon z_1)$$

$$= \varepsilon\left[k\xi - \frac{\partial z_0}{\partial T_0} - \varepsilon\left(\frac{\partial z_0}{\partial T_1} + \frac{\partial z_1}{\partial T_0}\right)\right] \tag{11}$$

A solution is sought by equating coefficients, on the right- and left-hand sides of Eq. (11), for each power of ε. This approach is valid because the functions z_n must hold for all values of ε and because sequences of ε are linearly independent.[11] For ε^0 and ε^1, this step yields the differential equations

$$\frac{\partial^2 z_0}{\partial T_0^2} + \omega^2 z_0 = 0 \tag{12a}$$

$$\frac{\partial^2 z_1}{\partial T_0^2} + \omega^2 z_1 = k\xi - \frac{\partial z_0}{\partial T_0} - 2\frac{\partial^2 z_0}{\partial T_0 \partial T_1} \tag{12b}$$

The solution of Eq. (12a) is known as the zero-order approximation, or the generating solution, and can be expressed as

$$z_0 = r(T_1)\sin[\omega T_0 + \phi(T_1)] \tag{13}$$

Note that the amplitude r and phase ϕ of the displacement z_0 vary slowly with time. Equation (13) can be rewritten as

$$z_0 = r(T_1)\sin(\omega_e T_0) \tag{14}$$

where

$$\omega_e = \frac{\mathrm{d}}{\mathrm{d}t}(\omega T_0 + \phi) = \left(\frac{\partial}{\partial T_0} + \varepsilon\frac{\partial}{\partial T_1}\right)(\omega T_0 + \phi) = \omega + \varepsilon\frac{\mathrm{d}\phi}{\mathrm{d}T_1} \tag{15}$$

Substituting Eq. (13) into Eq. (12b) yields

$$\frac{\partial^2 z_1}{\partial T_0^2} + \omega^2 z_1 = k\xi - \left(r + 2\frac{\mathrm{d}r}{\mathrm{d}T_1}\right)\omega\cos(\omega T_0 + \phi)$$

$$+ 2r\frac{\mathrm{d}\phi}{\mathrm{d}T_1}\omega\sin(\omega T_0 + \phi) \tag{16}$$

Harmonic Force Representation

Reference 3 showed that a harmonic approximation, in which only the fundamental term in the Fourier series expansion of the steady-state force variation ξ is retained, generally yields a response amplitude that is in good agreement with that for the multifrequency (nonharmonic) excitation. However, this harmonic approximation always underpredicts the true amplitude by an amount dependent on the salient ratio $f\Delta t/\zeta$; the agreement improves as this ratio increases.[3] Reference 7 further showed that the decomposition of the force variation into pulses and lags, as illustrated in Fig. 3, facilitates the conversion of the force variation into constant stiffness and damping terms in a modified equation of motion. The pulses in this decomposition represent the force variation for instantaneous

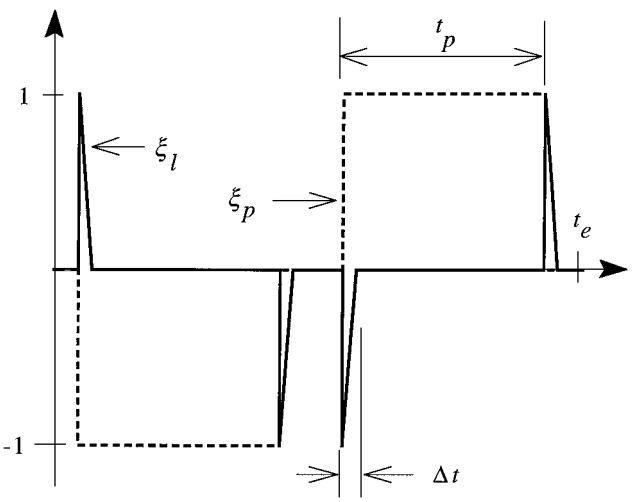

Fig. 3 Decomposition of aeroelastic coupling force variation into pulses and lags.

flow alternations, and the force lags account for the time that it actually takes the flow state to change.

Herein, the pulses and lags in each cycle are approximated by the fundamental term in their respective Fourier expansions, such that

$$\xi_p \cong -(4/\pi)\sin(\pi t_p/t_e)\sin(\omega_e T_0) \tag{17a}$$

$$\xi_l \cong (4\Delta t/t_e)\sin(\pi t_p/t_e)\cos(\omega_e T_0) \tag{17b}$$

where it is assumed that $\Delta t \ll t_e$. The pulses and lags, in other words, are smeared out over the response cycle in the form of a sine and cosine function, respectively.

In the transient problem under consideration, the instantaneous frequency ω_e (and period t_e) are functions of the slow timescale T_1, and the force changes initiate when the response reaches the critical displacement $z_{\rm cr}$. The pulse width t_p, therefore, depends on the displacement amplitude, and the term $\sin(\pi t_p/t_e)$ in Eqs. (17a) and (17b) must be written as an explicit function of r before proceeding. With reference to Fig. 2, the first time point in the response cycle at which the flow state changes yields the identity

$$z_{\rm cr} \cong r\sin(\omega_e t_a), \qquad \Delta t \ll t_e \tag{18}$$

where

$$t_e \cong 4t_a + 2t_p, \qquad \Delta t \ll t_e \tag{19}$$

With use of these expressions, it is easy to show that Eq. (17) can be expressed as

$$\xi_p \cong -(4/\pi)\left(\sqrt{r^2 - z_{\rm cr}^2}/r\right)\sin(\omega_e T_0), \qquad r \geq z_{\rm cr} \tag{20a}$$

$$\xi_l \cong (4\Delta t/t_e)\left(\sqrt{r^2 - z_{\rm cr}^2}/r\right)\cos(\omega_e T_0), \qquad r \geq z_{\rm cr} \tag{20b}$$

The requirement $r \geq z_{\rm cr}$ exists because the force changes only occur when the response exceeds the critical nose rotation value.

For consistency with the zero-order response approximation, Eq. (20) can be rewritten as

$$\xi_p \cong -(4/\pi)\left(\sqrt{r^2 - z_{\rm cr}^2}/r\right)\sin(\omega T_0 + \phi) + \mathcal{O}(\varepsilon), \qquad r \geq z_{\rm cr} \tag{21a}$$

$$\xi_l \cong 4f\Delta t\left(\sqrt{r^2 - z_{\rm cr}^2}/r\right)\cos(\omega T_0 + \phi) + \mathcal{O}(\varepsilon), \qquad r \geq z_{\rm cr} \tag{21b}$$

Substituting Eq. (21), as well as the definition of k, into Eq. (16) yields

$$\frac{\partial^2 z_1}{\partial T_0^2} + \omega^2 z_1 = \left[2r\frac{{\rm d}\phi}{{\rm d}T_1}\omega - \frac{4f}{\zeta}\frac{\sqrt{r^2 - z_{\rm cr}^2}}{r}\right]\sin(\omega T_0 + \phi) - \left[\omega\left(r + 2\frac{{\rm d}r}{{\rm d}T_1}\right) - \omega\frac{2f\Delta t}{\zeta}\frac{\sqrt{r^2 - z_{\rm cr}^2}}{r}\right]\cos(\omega T_0 + \phi) \qquad r \geq z_{\rm cr} \tag{22}$$

Response Amplitude and Frequency

Because of the sine and cosine terms on the right-hand side of Eq. (22), the solution z_1 grows without bound. However, the system is conservative and does not admit an unbounded response.[3] The secular terms on the right-hand side, therefore, must be suppressed by setting the bracketed expressions equal to zero, such that

$$2\frac{{\rm d}r}{{\rm d}T_1} + r - \frac{2f\Delta t}{\zeta}\frac{\sqrt{r^2 - z_{\rm cr}^2}}{r} = 0, \qquad r \geq z_{\rm cr} \tag{23a}$$

$$r\frac{{\rm d}\phi}{{\rm d}T_1} - \frac{1}{\pi\zeta}\frac{\sqrt{r^2 - z_{\rm cr}^2}}{r} = 0, \qquad r \geq z_{\rm cr} \tag{23b}$$

Equations (23a) and (23b) can be solved recursively; that is, Eq. (23a) provides a solution for the response amplitude r, whereas Eq. (23b) yields the phase ϕ, and consequently the frequency ω_e, once r has been defined.

General Solution

Equation (23a) can be rewritten as

$$\int \frac{r\,{\rm d}r}{r^2 - (2f\Delta t/\zeta)\sqrt{r^2 - z_{\rm cr}^2}} = \int \frac{-{\rm d}T_1}{2}, \qquad r \geq z_{\rm cr} \tag{24}$$

It can be shown that Eq. (24) has the solution

$$\left[\frac{(f\Delta t/\zeta)(1+u) - \sqrt{r^2 - z_{\rm cr}^2}}{(f\Delta t/\zeta)(1+u) - \sqrt{r_{\rm ic}^2 - z_{\rm cr}^2}}\right]^{(1+u)/2u} \times \left[\frac{\sqrt{r_{\rm ic}^2 - z_{\rm cr}^2} - (f\Delta t/\zeta)(1-u)}{\sqrt{r^2 - z_{\rm cr}^2} - (f\Delta t/\zeta)(1-u)}\right]^{(1-u)/2u} = e^{-\zeta\omega t} \qquad r_{\rm ic} \geq z_{\rm cr} \tag{25}$$

where

$$u = \sqrt{1 - \left(\frac{z_{\rm cr}}{f\Delta t/\zeta}\right)^2}, \qquad z_{\rm cr} \leq f\Delta t/\zeta \tag{26}$$

and εt has been substituted for T_1. The requirement $z_{\rm cr} \leq f\Delta t/\zeta$ makes sense because energy dissipation from structural damping in each cycle otherwise exceeds the energy input due to the force lags[3]; that is, the oscillation cannot sustain itself unless the normalized critical nose rotation is less than $f\Delta t/\zeta$.

Equations (15) and (23b) yield the following expression for the excitation frequency

$$\omega_e = \omega\left[1 + (2/\pi)\left(\sqrt{r^2 - z_{\rm cr}^2}/r^2\right)\right], \qquad r \geq z_{\rm cr} \tag{27}$$

where the value of r is determined from Eq. (25). Finally, the analytic results presented herein correspond to the zero-order response approximation defined by Eq. (14), where t is substituted for T_0, and r and ω_e are defined by Eqs. (25) and (27), respectively.

Improvement for Response Frequency

The accuracy of the general solution can be improved by retaining the first-order terms in the force expansions and in the time derivatives of z_0. It is easy to show that this revision changes all three occurrences of ω in the bracketed terms of Eq. (22) to ω_e. Hence, retaining the first-order terms does not affect the differential equation for the amplitude r [Eq. (23a)]. However, Eq. (23b), which establishes the phase ϕ, is updated to

$$r\left(1 + 2\zeta\frac{{\rm d}\phi}{{\rm d}T_1}\right)\frac{{\rm d}\phi}{{\rm d}T_1} - \frac{1}{\pi\zeta}\frac{\sqrt{r^2 - z_{\rm cr}^2}}{r} = 0, \qquad r \geq z_{\rm cr} \tag{28}$$

Solving Eq. (28) for ${\rm d}\phi/{\rm d}T_1$ and substituting the result into Eq. (15) yields the first-order response frequency

$$\omega_e = (\omega/2)\left[1 + \sqrt{1 + (8/\pi)\left(\sqrt{r^2 - z_{\rm cr}^2}/r^2\right)}\right], \qquad r \geq z_{\rm cr} \tag{29}$$

Limit Cycle Response

Limit cycle states correspond to periodic oscillation with a constant amplitude and frequency. Equation (25) shows that, as t tends to infinity, the response amplitude generally approaches

$$r_{\rm lc} = (f\Delta t/\zeta)\sqrt{2\left[1 + \sqrt{1 - \left(\frac{z_{\rm cr}}{f\Delta t/\zeta}\right)^2}\right]}, \qquad z_{\rm cr} \leq f\Delta t/\zeta \tag{30}$$

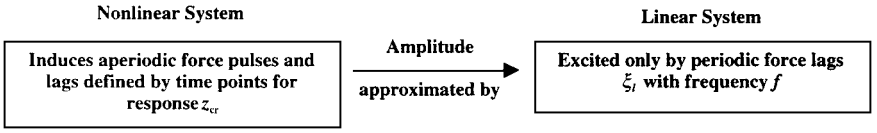

Fig. 4 Force pulses ξ_p do not affect response envelope.

Equation (25) also yields a constant response amplitude when the initial condition r_{ic} equals either the value from Eq. (30) or

$$r_u = (f\Delta t/\zeta)\sqrt{2\left[1-\sqrt{1-\left(\frac{z_{cr}}{f\Delta t/\zeta}\right)^2}\right]}, \qquad z_{cr} \le f\Delta t/\zeta \tag{31}$$

The states defined by Eqs. (30) and (31) represent the only equilibria from Eq. (25). This finding is consistent with the multifrequency solution of Ref. 3, which admits only two pulse widths and, hence, two steady-state response amplitudes, for any given z_{cr} value. With the half-angle trigonometric identity, it can further be shown that Eq. (30) is identical to the closed-form expression in Ref. 3 for the harmonic force approximation.

Equations (30) and (31) correspond, respectively, to the amplitude of a stable and an unstable limit cycle. It can be confirmed using Eq. (25) that, when the initial condition r_{ic} is slightly larger or smaller than r_{lc}, the resulting r value tends to r_{lc}. Similarly, it can be confirmed that r_{ic} values slightly larger and smaller than r_u yield a response that tends to r_{lc} and to rest, respectively.

Finally, it is proven in a later section that, provided $z_{cr} \neq 0$, the state of rest is a third equilibrium. By Rolle's theorem, the product of the concavity of the potential for adjoining equilibria must be negative. Hence, the limit cycles defined by Eqs. (31) and (30), which encircle the state of rest (stable fixed point), must be unstable and stable, respectively.

Flow State Changes at Zero Critical Deflection

The special case in which the flow state changes at zero critical deflection is of interest because this condition produces the largest limit cycle response.[3] As discussed in a later section, a subcritical Hopf bifurcation also occurs at $z_{cr} \equiv 0$.

Equation (26) shows that u equals unity when $z_{cr} \equiv 0$; hence, Eq. (25) reduces to the simple expression

$$r = e^{-\zeta\omega t}(r_{ic} - r_{lc}) + r_{lc} \tag{32}$$

where

$$r_{lc} = 2f\Delta t/\zeta \tag{33}$$

It is obvious from Eq. (32) that the response converges to the limit cycle amplitude for arbitrary values of the initial condition r_{ic}. Equation (32) also shows that if the initial displacement equals precisely $2f\Delta t/\zeta$, the response is steady state for all time t. Equation (30) corroborates this limit cycle amplitude. Finally, Eq. (31) confirms that the unstable limit cycle corresponds to a state of rest for this special case; that is, the response tends to $2f\Delta t/\zeta$ even for initial response values equal to zero.

Equation (32) can be rewritten as

$$r = (A/2\zeta)(1 - e^{-\zeta\omega t}) + r_{ic}e^{-\zeta\omega t} \tag{34}$$

where

$$A = 4f\Delta t \tag{35}$$

It can be shown that Eq. (34) is an approximate expression for the resonant response of a single-degree-of-freedom linear system[12] subjected to a sine force of amplitude A. When $z_{cr} \equiv 0$, and provided the excitation frequency is identical to the system natural frequency, A equals the fundamental term in a Fourier series expansion of the force lags. This means that, for zero critical deflection, the amplitude of the nonlinear response can be approximated by that for a linear system excited by periodic force lags with frequency f. This leads to the interesting conclusion, summarized in Fig. 4, that the force pulses ξ_p (shown in Fig. 3) do not affect the response envelope.

Effective System Damping

It is popular in the analysis of fluid–structure interaction problems to treat flow-induced forces as a modification to the system frequency and damping.[13] The conversion of the alternating flow forces in the current problem into equivalent stiffness and damping terms was extensively investigated in Ref. 7 for steady-state oscillation. These effects are explored in this section to provide assessments during the evolution of the response to the limit cycle state.

Equation (1) can be written as[7]

$$\ddot{z}(t) + 2\omega(\zeta + \dot{n})\dot{z}(t) + \omega^2(1+n)z(t) = 0 \tag{36}$$

where

$$\dot{n} = -\omega\xi_l/2\dot{z} \tag{37a}$$

$$n = -\xi_p/z \tag{37b}$$

That is, the force lags modify the system damping, whereas the force pulses affect the system frequency. From Eq. (13) it is evident that the response velocity is approximated by

$$\dot{z} = r\omega\cos(\omega T_0 + \phi) + \mathcal{O}(\varepsilon) \tag{38}$$

Substituting Eqs. (21b) and (38) into Eq. (37a) yields

$$\dot{n} = -2f\Delta t\left(\sqrt{r^2 - z_{cr}^2}/r^2\right) \tag{39}$$

Similarly, substituting Eqs. (13) and (21a) into Eq. (37b) yields

$$n = (4/\pi)\left(\sqrt{r^2 - z_{cr}^2}/r^2\right) \tag{40}$$

Equation (36) indicates that the effective system frequency is defined by

$$\omega_e = \omega\sqrt{1+n} = \omega\left[1 + (2/\pi)\left(\sqrt{r^2 - z_{cr}^2}/r^2\right)\right] + \mathcal{O}(n^2) \tag{41}$$

which corroborates Eq. (27).

The net damping indicated by the sum $\zeta + \dot{n}$ in Eq. (36) is given by

$$\zeta_e = \zeta + \dot{n} = \zeta\left[1 - (2f\Delta t/\zeta)\left(\sqrt{r^2 - z_{cr}^2}/r^2\right)\right] \tag{42}$$

Note, however, that Eq. (36) can be interpreted as the equation of motion for a linear oscillator with natural frequency ω_e. Equation (42) then must be normalized using Eq. (41) to yield the damping value for a single-degree-of-freedom system with this natural frequency.

Equations (39) and (40) vary with the slow timescale T_1, not the fast timescale $t = T_0$. The aerodynamic stiffness and damping expressions do not vary significantly within any given response cycle because the harmonic approximation linearizes Eq. (1) (Ref. 7). Aerodynamic stiffness and damping values consistent with the multifrequency (nonharmonic) excitation, however, are not constant within a response cycle even for steady-state oscillation.[7]

The force term has been eliminated from Eq. (36) through the introduction of frequency and damping modifications. Responses computed using Eq. (36), therefore, occur strictly through free vibration given initial values of displacement and velocity. For negative, positive, and zero damping values, the response envelope grows, decays, and is constant, respectively. Substitution of Eqs. (30) and (31) into Eq. (42) confirms that the effective system damping value equals zero for both the stable and unstable limit cycle states.

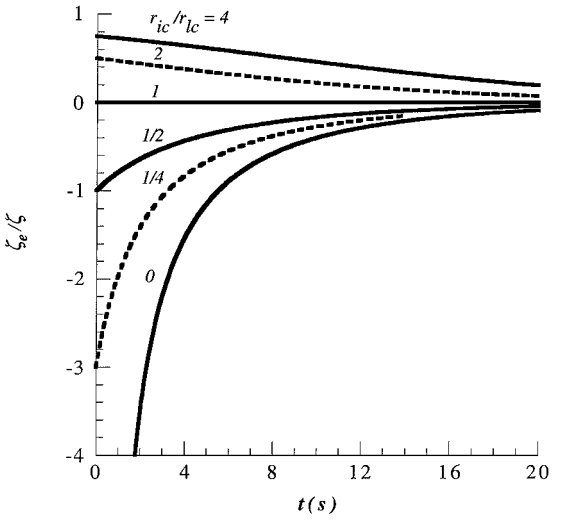

Fig. 5 Effective system damping ($f = 2$ Hz, $\zeta = 1\%$, and $z_{cr} = 0$).

Effective system damping can be further investigated by examining the special case $z_{cr} \equiv 0$. Making use of Eq. (32) it is easy to show that Eq. (42) yields

$$\frac{\zeta_e}{\zeta} = \frac{1 - r_{ic}/r_{lc}}{1 - r_{ic}/r_{lc} - e^{\zeta\omega t}} \qquad z_{cr} \equiv 0 \qquad (43)$$

Results from Eq. (43) computed for a 2-Hz bending mode with 1% of critical structural damping are plotted in Fig. 5. When $r_{ic} > r_{lc}$, effective system damping has a positive value, reflecting that the free vibration decays toward the limit cycle amplitude. Similarly, when $r_{ic} < r_{lc}$, Eq. (43) yields a negative value because the response amplitude must increase during free vibration to reach r_{lc}. Because of the exponential term in the denominator, Eq. (43) converges to zero for all initial conditions.

The large undamping apparent in Fig. 5 for low values of r_{ic}/r_{lc} merely indicates that the initial response is small compared to the limit cycle amplitude and that the response must grow significantly to reach this limiting value. Large undamping does not imply, as other investigators have concluded, that launch vehicle aeroelastic coupling may induce responses that diverge to infinity. It is obvious from Eq. (43) that the effective system damping value can be extremely negative even when the limit cycle amplitude is small and of little consequence to the system. Hence, the conversion of alternating flow forces into aerodynamic stiffness and damping terms is not generally recommended for the current problem.

Structure of the Solution Space

Effect of Critical Response Value

The effect of z_{cr} on the response amplitude is investigated further in this section. Figure 6 illustrates the structure of the solution space as a function of this control parameter. The boundary of the dark cone represents the amplitude of the unstable limit cycle, defined by Eq. (31). The outer surface of the body in Fig. 6 represents the amplitude of the stable limit cycle, defined by Eq. (30). Initial conditions that lie outside of the cone yield a response that tends to the body's outer surface, whereas initial conditions that lie inside of the cone yield a response that tends to rest.

The boundary of the cone and the body's outer surface meet at $z_{cr} = f\Delta t/\zeta$; that is, the unstable and stable limit cycles have the same amplitude when $z_{cr} = f\Delta t/\zeta$. Beyond this z_{cr} threshold, dissipation from structural damping exceeds the energy input caused by the flowfield time lag.[3] A stable limit cycle, therefore, does not exist when $z_{cr} > f\Delta t/\zeta$, and the response tends to rest regardless of the initial conditions. Hence, the solution space terminates at $z_{cr} = f\Delta t/\zeta$. Finally, provided that $z_{cr} \le f\Delta t/\zeta$, initial conditions that lie outside of the body yield a response that tends to the outer surface.

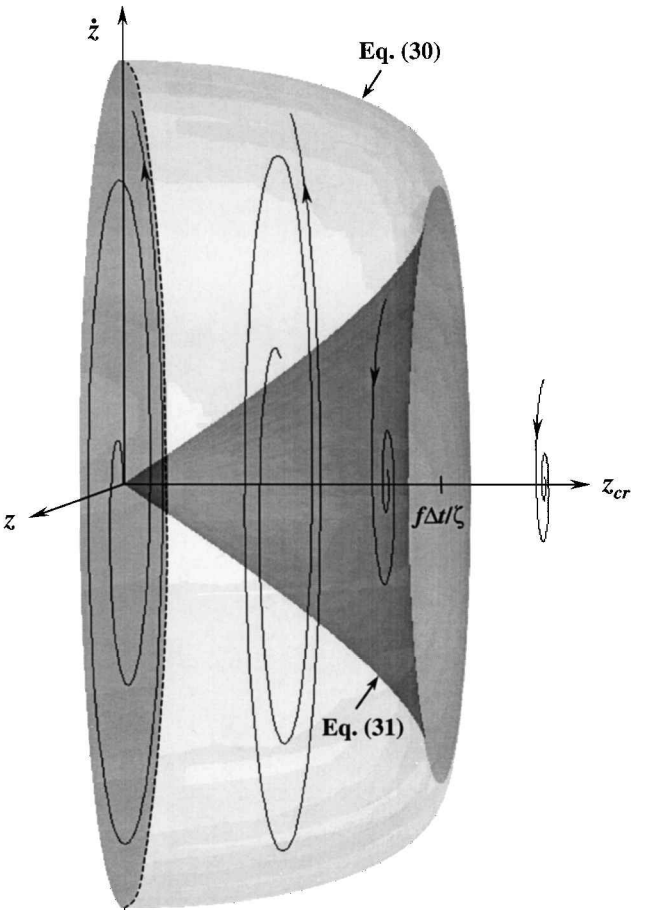

Fig. 6 Bifurcation diagram for control parameter z_{cr}.

Hopf Bifurcation

For any nonzero value of z_{cr}, there is a response amplitude below which the force variation ξ does not exist. Near the state of rest, therefore, the equation of motion reduces to that for free vibration of a single-degree-of-freedom system with frequency ω and structural damping ζ. The eigenvalues of the Jacobian matrix[14] at the fixed point $(z, \dot{z}) = (0, 0)$ are then defined by

$$\lambda = -\zeta\omega \pm i\omega\sqrt{1 - \zeta^2}, \qquad z_{cr} \neq 0 \qquad (44)$$

Equation (44) yields a complex conjugate pair with $\mathrm{Re}\,\lambda < 0$. The fixed point $(z, \dot{z}) = (0, 0)$ is, therefore, asymptotically stable provided $z_{cr} \neq 0$ (Ref. 14).

For the special case $z_{cr} \equiv 0$, the force variation ξ is created ex nihilo because the flow state changes even when the system is initially at rest. It can be shown using Eq. (36) that the eigenvalues of the Jacobian matrix for the fixed point $(z, \dot{z}) = (0, 0)$ in this case are given by

$$\lambda = -\zeta_e\omega \pm i\omega\sqrt{(\omega_e/\omega)^2 - \zeta_e^2}, \qquad z_{cr} \equiv 0 \qquad (45)$$

where

$$\zeta_e = \zeta(1 - r_{lc}/r), \qquad r_{lc} = 2f\Delta t/\zeta \qquad (46a)$$

$$\omega_e = \omega\sqrt{1 + 4/\pi r} \qquad (46b)$$

Equation (46a) indicates that a bending mode that is initially at rest will have an effective damping value that becomes negative when the launch vehicle enters the transonic regime. The real part of the eigenvalues of the Jacobian matrix, consequently, changes from negative to positive as z_{cr} approaches zero. Eigenvalues that cross the imaginary axis in the complex plane are indicative of a Hopf bifurcation,[14] and the vanishing of linearized damping is typical for oscillators that exhibit this loss of stability.[14]

Figure 6 shows that as z_{cr} decreases, the unstable limit cycle shrinks around the stable fixed point $(z, \dot{z}) = (0, 0)$. At $z_{cr} \equiv 0$, the unstable limit cycle has zero amplitude, and the stable equilibrium point becomes unstable. As shown by the dark plane, after the bifurcation, trajectories that used to remain near the origin now must jump to the large-amplitude stable limit cycle. This situation is emblematic of subcritical Hopf bifurcation, or Hopf bifurcation in its catastrophic form.[14]

Comparisons with Numerical Results

The preceeding analytic expressions are compared in this section with results from a numerical solution of the nonlinear equation of motion. The algorithm computes the response over each piecewise linear force segment. The time point at which the displacement reached $\pm z_{cr}$ is established, and the force history is augmented with the appropriate piecewise linear segment. This time-marching numerical solution, therefore, maintains the discrete changes dictated by Fig. 2.

The numerical solution was established for a 2-Hz bending mode with 1% of critical structural damping. The flowfield time lag was taken as 10 ms, and the normalized critical deflection and initial displacement equaled 0.5 and 1, respectively. The response displacement and force variation for the numerical solution during the first 4 s are shown in Fig. 7. Note that the force and response are out of phase, as required for self-sustained oscillation.[3]

The response envelope is compared in Fig. 8 with the multiple-scales solution from Eqs. (25) and (32). Equation (25) underestimates the response amplitude because the harmonic approximation of the force variation was used in its derivation. The results from Eq. (32) correspond to $t_a = 0$, that is, to elimination of the force dead zones in Fig. 2; the response amplitude is greatest for this limiting case.[3] Figure 8 illustrates that, for this example, setting z_{cr} equal to zero generally compensates for the underprediction due to the harmonic approximation.

Results from Eqs. (27) and (29), computed using the response amplitude from Eq. (25), are plotted in Fig. 9. The numerical results included for comparison are based on the time interval for each response cycle. As expected, the first-order approximation improves the accuracy of the multiple-scales solution. Curves of normalized frequency for $z_{cr} = 0$ are almost identical to those for $z_{cr} = 0.5$ and, consequently, are not shown.

Figures 8 and 9 illustrate that the multiple-scales solution is in good agreement with the numerical result. For all time t, the difference between the numerical and analytic response amplitudes does not exceed 5%. This agreement is remarkable because the value of ε for this example, 0.25, is not very small.

The amplitude and normalized frequency for the limit cycle state are included in Figs. 8 and 9 for comparison. Closed-form expressions presented in Ref. 3 for multifrequency excitation yield a limit

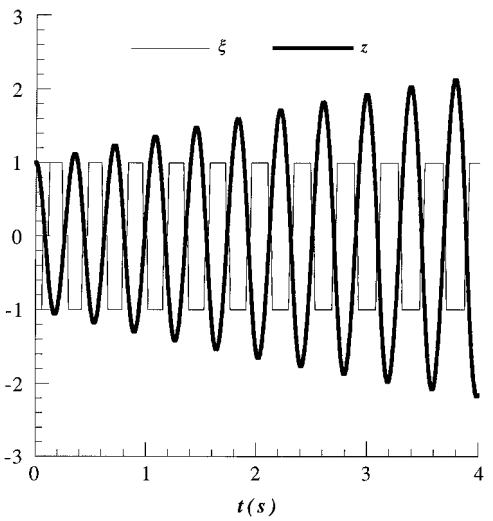

Fig. 7 Numerical solution of nonlinear equation of motion ($f = 2$ Hz, $\zeta = 1\%$, $\Delta t = 10$ ms, $z_{cr} = 0.5$, and $z_{ic} = 1$).

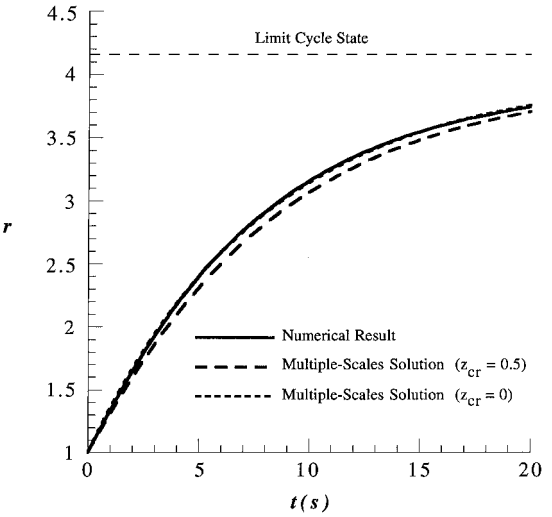

Fig. 8 Envelope of transient response amplitude ($f = 2$ Hz, $\zeta = 1\%$, $\Delta t = 10$ ms, $z_{cr} = 0.5$, and $z_{ic} = 1$).

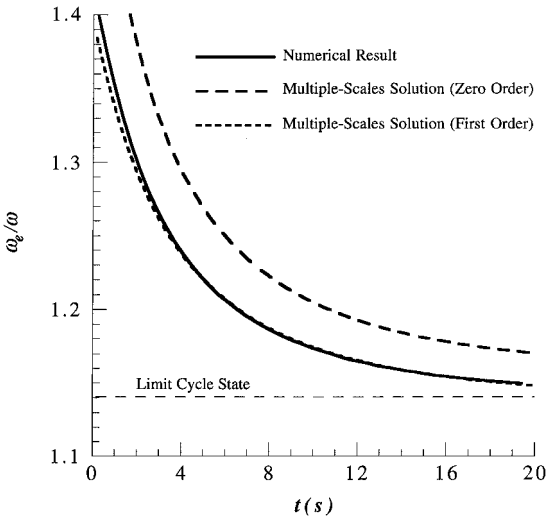

Fig. 9 Normalized transient response frequency ($f = 2$ Hz, $\zeta = 1\%$, $\Delta t = 10$ ms, $z_{cr} = 0.5$, and $z_{ic} = 1$).

cycle amplitude and normalized frequency equal to 4.16 and 1.14, respectively. These values are in excellent agreement with those for the converged numerical solution. Equation (30) indicates that the limit cycle amplitude from the harmonic approximation equals 3.97. The corresponding normalized frequency from Eq. (29) equals 1.14. As expected, the amplitude is slightly lower than the numerical or multifrequency analytic result.

Equation (31) indicates that the unstable limit cycle amplitude equals 0.50. Because the initial displacement exceeds this value, the envelope of the response amplitude increases and converges to the stable steady state. Finally, Eq. (42) indicates that effective system damping equals -2.5% at response initiation for this example.

Initial Response Envelope

From the example considered in the preceding section, it is clear that it can take a considerable amount of time for the response to reach the steady-state limit. Because launch vehicles fly only briefly in the transonic regime, the initial response growth is investigated further in this section. The simple expression for the case $z_{cr} \equiv 0$ is used heuristically. The derivative of Eq. (32) shows that the rate of increase in the response envelope is largest when the initial displacement equals zero. For this case, Eq. (32) can be rewritten as

$$r/\Delta t = (2f/\zeta)(1 - e^{-2\pi f \zeta t}) \tag{47}$$

Results from Eq. (47) are plotted in Fig. 10.

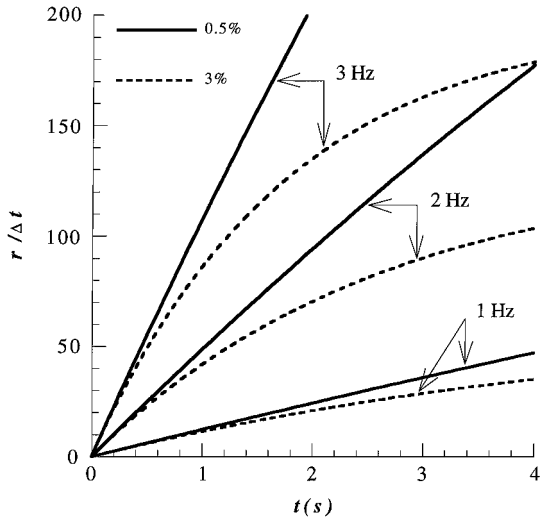

Fig. 10 Multiple-scales solution for ranges of frequency and damping ($z_{cr} = 0$ and $z_{ic} = 0$).

The frequency of the fundamental bending mode for launch vehicles is generally less than 3 Hz. Similarly, structural damping values for bending modes generally fall within the range shown in Fig. 10. The curves are truncated at 4 s because launch vehicles typically require less than 4 s to fly through the Mach number region for flow state alternations. If the vehicle acceleration is roughly constant during the transonic regime, the maximum time for force–response coupling can be approximated by

$$t_{\max} = c\Delta M/\ddot{x} \tag{48}$$

where the Mach number interval ΔM is less than 0.1 for a wide range of payload fairing nose cone angles.[2] Using $\Delta M \approx 0.1$ with $c \approx$ 1000 ft/s yields $t_{\max} < 3$ s for a 1-g absolute vehicle acceleration.

Figure 10 shows that the response envelope does not approach the limit cycle state within 4 s, unless the bending mode has relatively high values of both frequency and damping. For example, when $f = 3$ Hz and $\zeta = 3\%$, the response envelope reaches 90% of the limit cycle amplitude. For lower values of frequency and damping, this percentage is much smaller.

Note that when the product $f\zeta t$ is low, the curves in Fig. 10 are approximately linear. This linearity corresponds to retaining only the first two terms in the expansion of the exponential in Eq. (47), which leads to the relationship

$$r < (4\pi f^2 \Delta t)t \tag{49}$$

Because the response for $z_{cr} > 0$ is bounded by that for $z_{cr} \equiv 0$, Eq. (49) is valid for all values of the critical nose rotation. This expression also serves as a bound for the special case in which flow state changes occur on only one side of the payload fairing; that is, the two-sided changes considered in the current problem induce larger response amplitudes than do one-sided changes.

Equation (49) emphasizes that proper definition of the flowfield time lag is critical for estimation of the bending mode response from launch vehicle aeroelastic coupling. For example, a 2-Hz mode experiencing aeroelastic coupling for 2 s must be associated with a 10-ms time lag for the normalized response amplitude to exceed unity. This result means that a 10-ms time lag is required for the response to exceed that for static application of the alternating flow forces. Reference 4 showed that assumptions regarding the mechanism that induces the flow state alternations can lead to disparate time lag values and concluded that further work is needed to characterize the aeroelastic nature of the flow changes.

Conclusions

The multiple-scales approximation for the idealized force–response coupling yields closed-form expressions that agree well with numerical solutions of the governing nonlinear differential equation. These analytic expressions based on the phenomenological model show that the maximum response amplitude during launch vehicle aeroelastic coupling is critically dependent on the flowfield time lag, the period that the launch vehicle spends in the transonic region, and the product of the bending mode natural frequency and structural damping values. Because launch vehicles fly quickly through the transonic region, the low values of natural frequency and structural damping typical for fundamental bending modes generally preclude convergence of the response to the limit cycle state.

It can also be concluded that the concept of instability based strictly on the existence of negative values of effective system damping overlooks the important distinction that, even given an unlimited amount of time to achieve convergence, the response amplitude for steady-state launch vehicle aeroelastic coupling may be small. Indeed, instability implied by negative effective damping simply means that the launch vehicle response grows from an initial state. The amplitude of the response at the conclusion of the transonic regime is clearly a more important measure than the effective damping value at initiation of the flow state changes.

References

[1]Robertson, J. E., and Chevalier, H. L., "Characteristics of Steady-State Pressures on the Cylindrical Portion of Cone-Cylinder Bodies at Transonic Speeds," Arnold Engineering Development Center, AEDC TDR-63-104, Tullahoma, TN, Aug. 1963.

[2]Chevalier, H. L., and Robertson, J. E., "Pressure Fluctuations Resulting from an Alternating Flow Separation and Attachment at Transonic Speeds," Arnold Engineering Development Center, AEDC TDR-63-204, Tullahoma, TN, Nov. 1963.

[3]Dotson, K. W., Baker, R. L., and Sako, B. H., "Launch Vehicle Self-Sustained Oscillation from Aeroelastic Coupling Part 1: Theory," *Journal of Spacecraft and Rockets*, Vol. 35, No. 3, 1998, pp. 365–373.

[4]Dotson, K. W., Baker, R. L., and Bywater, R. J., "Launch Vehicle Self-Sustained Oscillation from Aeroelastic Coupling Part 2: Analysis," *Journal of Spacecraft and Rockets*, Vol. 35, No. 3, 1998, pp. 374–379.

[5]Moss, G. F., and Pierce, D., "The Dynamic Response of Wings in Torsion at High Subsonic Speeds," *Unsteady Airloads in Separated and Transonic Flow*, CP-226, AGARD, 1977, pp. 4-1–4-21.

[6]Steger, J. L., and Bailey, H. E., "Calculation of Transonic Aileron Buzz," *AIAA Journal*, Vol. 18, No. 3, 1980, pp. 249–255.

[7]Dotson, K. W., Baker, R. L., and Sako, B. H., "Launch Vehicle Buffeting with Aeroelastic Coupling Effects," *Journal of Fluids and Structures*, Vol. 14, No. 8, 2000, pp. 1145–1171.

[8]Chen, S.-H., and Dotson, K. W., "A Time-Marching Aeroelastic Analysis of Launch Vehicles in Transonic Flow," The Aerospace Corp., Rept. ATR-2000(8424)-1, Los Angeles, 2000.

[9]Azevedo, J. L. F., "Aeroelastic Analysis of Launch Vehicles in Transonic Flight," *Journal of Spacecraft and Rockets*, Vol. 26, No. 1, 1989, pp. 14–23.

[10]Cunningham, A. M., Jr., and Meijer, J. J., "Semi-Empirical Unsteady Aerodynamics for Modeling Aircraft Limit Cycle Oscillations and Other Non-Linear Aeroelastic Problems," *International Forum on Aeroelasticity and Structural Dynamics 1995*, Vol. 2 (A95-42613 11-39), Royal Aeronautical Society, London, 1995, pp. 74.1–74.14.

[11]Nayfeh, A. H., *Perturbation Methods*, 1st ed., Wiley, New York, 1973, pp. 228–307.

[12]Clough, R. W., and Penzien, J., *Dynamics of Structures*, 1st ed., McGraw–Hill, New York, 1975, pp. 60–62.

[13]Dowell, E. H. (ed.), *A Modern Course in Aeroelasticity*, 3rd ed., Kluwer Academic, Boston, 1995, pp. 472–532.

[14]Thompson, J. M. T., and Stewart, H. B., *Nonlinear Dynamics and Chaos*, 1st ed., Wiley, New York, 1986, pp. 111–121.

R. B. Malla
Associate Editor